STUDY OF INERTIA EFFECTS ON DYNAMIC TWO-PHASE OSCILLATION PHENOMENA

Ruspini, L.C.^{a,1}

^aDepartment of Energy and Process Engineering. Faculty of Engineering Science and Technology, Norwegian University of Science and Technology leonardo.c.ruspini@ntnu.no

Abstract

Thermal-hydraulic instabilities and oscillations are unwanted effects which can result in severe damages of two phase flow systems. The most common dynamic two-phase flow instability, namely density wave oscillations, is studied. The stability influence of external parameters such as the inertia of the subcooled liquid before the heated channel and the inertia of the fluid after the heated channel are analyzed. Non-dimensional stability maps, as a function of the subcooling and the phase-change numbers are constructed. The influence of the inertia components on the stability boundaries is studied and characterized. The study is performed by modeling a single boiling channel using a homogeneous model. A compressible transient model describes the evolution of the flow and pressure in the non-heated regions. Finally the problem is solved using a high-order method, allowing to describe the involved phenomena with high accuracy and avoiding the numerical diffusivity, characteristic of low order methods. The implementation of wavelet decomposition in the analysis of the simulation results is also described.

1. Introduction

The occurrence of oscillations and instabilities may cause severe damages in many industrial systems, such as heat exchangers, nuclear reactors, re-boilers, steam generators, thermal-siphons, etc. These phenomena induced in boiling flows are of relevance for the design and operation of two-phase systems. Consequently the stability in thermo-hydraulic variables such as mass flux, pressure and temperature should be studied in detail to better understand and characterize the conditions for the occurrence of these phenomena.

A theoretical description of density waves oscillations (DWO) can be found in [7, 12, 15]. Nevertheless these works seem to differ in the description of high-order DWO. In one hand, [15] describes experimentally the occurrence of high-order and normal DWO, while in the other hand [7] and subsequent works do not observe high-order oscillations in experiments or analytical descriptions. Moreover in [3, 10, 9, 1, 8] several aspects of the classical description and the modeling of DWO are critically discussed. The nature of the phenomena that influence the occurrence of DWO for different regimes is thoroughly analyzed. Nevertheless none high-order DWO are described in these last works either.

The purpose of this work is to analyze the influence of the inertia in the different parts a boiling system. A non-dimensional stability analysis is presented. The behavior of the system for different regions and different parameter is studied. The conditions for the occurrence of high-order DWO is also analyzed.

2. Model

The thermo-hydraulic system used to study this kind of instabilities consists of two constant pressure tanks, two valves, a heated section and two pipe lines, as shown in Figure 1. In this model the pressure

¹Tel: +47 73593985, Fax: +47 73593491.

Table 1: Nomenclature

	Lowercase	G	mass flux
h	specific enthalpy	K	valve constant
f	Darcy friction factor	L	pipe length
t	time coordinate	P	pressure
v	specific volume	P_H	wet perimeter
\boldsymbol{x}	themodynamic quality	Q	constant heat source
z	space coordinate	T	temperature
ρ	density	Subscrip	ots
	Uppercase	in	inlet
A_{xs}	cross section area	out	outlet
D_H	hydraulic diameter	TS	test section

difference between both tanks acts as the driving force and, according to the K_{in} valve opening, the external characteristic ($\Delta P \ vs. \ G$) results in a quadratic decreasing curve. The implemented model is based on the following assumptions,

- One-dimensional model.
- Thermodynamic equilibrium conditions.
- Two-phase homogeneous model [8].
- Colebrook pressure drop correlation in the single phase region and two-phase Müller-Steinhagen and Heck pressure drop correlation for two-phase flow region [13].

The mathematical description of the external system is based on an adiabatic incompressible model. The momentum conservation equations for the external system can be expressed as

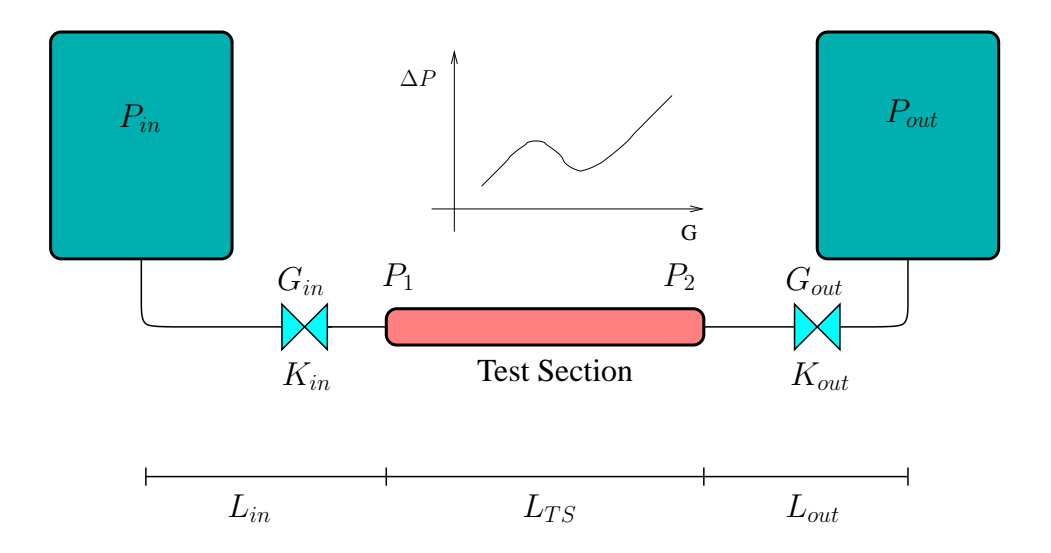


Figure 1: Scheme of the implemented model.

$$\dot{G}_{in} = \left[P_{in} - P_1 - (K_{in} + 1) \frac{G_{in}^2}{2\rho_{in}} \right] \frac{1}{L_{in}}$$
(1)

$$\dot{G}_{out} = \left[P_2 - P_{out} - (K_{out} - 1) \frac{G_{out}^2}{2\rho_{out}} \right] \frac{1}{L_{out}}$$
 (2)

The mathematical model used to describe the evolution of the heated section is based on the mass, momentum and energy conservation. They can be expressed as

$$\frac{\partial \rho}{\partial t} + \frac{\partial G}{\partial z} = 0 \tag{3}$$

$$\frac{\partial G}{\partial t} + \frac{\partial}{\partial z} \left(\frac{G^2}{\rho} \right) + \frac{\partial P}{\partial z} + \frac{f}{D_H} \frac{G^2}{2\rho} = 0 \tag{4}$$

$$\frac{\partial \rho h}{\partial t} + \frac{\partial Gh}{\partial z} = Q \frac{P_H}{A_x} \tag{5}$$

The pressure drop in the valves is calculated using a pressure drop concentrated value, K_i , for each valve. Friction losses are neglected in the energy equation. Finally the friction factor, eq. (4), is given by the known Colebrook correlation for the single phase regions, liquid or gas [14], and by Müller-Steinhagen and Heck correlation for the two-phase region [13].

3. Numerical approximation

The introduction of a significant diffusion by low-order methods can affect the numerical solution, describing inaccurately the modeled problem. High-order discretization reduces the numerical diffusion. The necessity of solving thermal-hydraulic problems with high accuracy is analyzed in [4, 11].

In a general case the least squares formulation is based on the minimization of a norm–equivalent functional. For simplicity, the system of equations can be represented as

$$\mathcal{L}\mathbf{u} = \mathbf{g} \quad in \ \Omega \tag{6}$$

$$\mathcal{B}\mathbf{u} = \mathbf{u}_{\Gamma} \quad on \ \Gamma \subset \partial\Omega \tag{7}$$

with \mathcal{L} a linear partial differential operator and \mathcal{B} the trace operator. We assume that the system is well–posed and the operator $(\mathcal{L}, \mathcal{B})$ is a continuous mapping between the function space $X(\Omega)$ onto the space $Y(\Omega) \times Y(\Gamma)$.

The norm equivalent functional becomes

$$\mathcal{J}(\mathbf{u}) \equiv \frac{1}{2} \parallel \mathcal{L}\mathbf{u} - \mathbf{g} \parallel_{Y(\Omega)}^{2} + \frac{1}{2} \parallel \mathcal{B}\mathbf{u} - \mathbf{u}_{\Gamma} \parallel_{Y(\Gamma)}^{2}$$
 (8)

Based on variational analysis, the minimization statement is equivalent to:

$$\lim_{\epsilon \to 0} \frac{d}{d\epsilon} \mathcal{J}(\mathbf{u} + \epsilon \, \mathbf{v}) = 0 \quad \forall \, \mathbf{u} \in X(\Omega)$$
(9)

Hence, the necessary condition for the minimization of \mathcal{J} is equivalent to: Find $f \in X(\Omega)$ such that

$$\mathcal{A}(\mathbf{u}, \mathbf{v}) = \mathcal{F}(\mathbf{v}) \quad \forall \mathbf{v} \in X(\Omega)$$
 (10)

with

$$\mathcal{A}(\mathbf{u}, \mathbf{v}) = \langle \mathcal{L}\mathbf{u}, \mathcal{L}\mathbf{v} \rangle_{Y(\Omega)} + \langle \mathcal{B}\mathbf{u}, \mathcal{B}\mathbf{v} \rangle_{Y(\Gamma)}$$
(11)

$$\mathcal{F}(\mathbf{v}) = \langle \mathbf{g}, \mathcal{L}\mathbf{v} \rangle_{Y(\Omega)} + \langle \mathbf{u}_{\Gamma}, \mathcal{B}\mathbf{v} \rangle_{Y(\Gamma)}$$
(12)

$$\mathcal{A}(\mathbf{v}_h, \mathbf{v}_h)\mathbf{u}_h = \mathcal{F}(\mathbf{v}_h) \quad \forall \mathbf{v}_h \in X_h(\Omega_h)$$
(13)

where $A: X \times X \to \mathbb{R}$ is a symmetric, continuous bilinear form, and $\mathcal{F}: X \to \mathbb{R}$ a continuous linear form. The introduction of the boundary residual allows the use of spaces $X(\Omega)$ that are not constrained to satisfy the boundary conditions. The boundary terms can be omitted and the boundary conditions must be enforced strongly in the definition of the space $X(\Omega)$. Finally, the searching space is restricted to a finite dimensional space such that $\mathbf{u}_h \in X_h(\Omega) \subset X(\Omega)$.

3.1. Numerical description of the internal problem

From equations (3-5) it is possible to see that the system is non-linear (quasi-linear). For that reason it is necessary to find a linear form for this set of equations in order to use LSSM (Least Square Spectral Method). Non-linear effects and the coupling between internal and the external systems are considered by implementing an iterative Picard loop. The linearization of the system described in Eqs. (3-5) results in

$$\frac{\partial \rho^*}{\partial t} + \frac{\partial G}{\partial z} = 0 \tag{14}$$

$$\frac{\partial G}{\partial t} + \frac{\partial}{\partial z} \left(\frac{G^{*2}}{\rho^*} \right) + \frac{\partial P}{\partial z} + \frac{f}{D_H} \frac{G^{*2}}{2\rho^*} = 0 \tag{15}$$

$$\frac{\partial \rho^* h}{\partial t} + \frac{\partial G^* h}{\partial z} = Q \frac{P_H}{A_x} \tag{16}$$

where G^* and ρ^* correspond to the old values of flow and density respectively. Hence, using the operator description of eq. (6), it is possible to rewrite the linearized system as

$$\mathcal{L}_{int} = \begin{cases} \frac{\partial \bullet}{\partial z} & 0 & 0 \\ \frac{\partial}{\partial t} & \frac{\partial \bullet}{\partial z} & 0 \\ 0 & 0 & \rho^* \frac{\partial \bullet}{\partial t} + G^* \frac{\partial \bullet}{\partial z} \end{cases}$$

$$(17)$$

$$\mathbf{g}_{int} = \left\{ -\frac{\partial \rho^*}{\partial z} \left(\frac{G^{*2}}{\rho^*} \right) - \frac{f}{D_H} \frac{G^{*2}}{2\rho^*} \right\}$$

$$Q \frac{P_H}{A_T}$$
(18)

$$\mathbf{u}_{int} = \left\{ \begin{array}{c} G \\ P \\ h \end{array} \right\} \tag{19}$$

and the operator \mathcal{B}_{int} is the matrix where the corresponding initial and boundary nodes are set to one and the \mathbf{u}_{Γ} corresponds to the initial values for flow, pressure and enthalpy. In x=0 the boundary conditions for enthalpy, flow are added to the vector \mathbf{u}_{Γ} , while the boundary condition for the pressure is set at x=1.

3.2. Numerical description of the external problem

In contrast with the internal system, the external system is solved just as a function of the time (t). The operator description of this system, Eqs. (1-2)

$$\mathcal{L}_{ext} = \left\{ \begin{array}{cc} \frac{\partial \bullet}{\partial t} & 0\\ 0 & \frac{\partial \bullet}{\partial t} \end{array} \right\}$$
 (20)

$$\mathbf{g}_{ext} = \begin{cases} \left[P_{in} - P_1^* - (K_{in} + 1) \frac{(G_{in}^*)^2}{2\rho_{in}} \right] \frac{1}{L_{in}} \\ \left[P_2^* - P_{out} - (K_{out} - 1) \frac{(G_{out}^*)^2}{2\rho_{out}^*} \right] \frac{1}{L_{out}} \end{cases}$$
(21)

$$\mathbf{u}_{ext} = \left\{ \begin{array}{c} G_{in} \\ G_{out} \end{array} \right\} \tag{22}$$

where the * values correspond to the values of the variables in the previous step. The values of P_{in} and G_{out} are taken as initial boundary conditions.

3.3. Spectral element approximation

The computational domain Ω is divided into N_e non-overlapping sub-domains Ω_e of diameter h_e , called spectral elements, such that

$$\Omega = \bigcup_{e=1}^{N_e} \Omega_e, \qquad \Omega_e \cap \Omega_l = \emptyset, \quad e \neq l$$
(23)

The global approximation in Ω , \mathbf{u}_h , is constructed by gluing the local approximations \mathbf{u}_h^e , i.e.

$$\mathbf{u}_h = \bigcup_{e=1}^{N_e} \mathbf{u}_h^e \tag{24}$$

The local approximation solution \mathbf{u}_h^e can be expressed like

$$\mathbf{u}_{h}^{e}(x,t) = \sum_{i=0}^{N_{1}} \sum_{j=0}^{N_{2}} u_{ij}^{e} \, \varphi_{i}(x) \, \varphi_{j}(t), \quad \text{with } u_{ij}^{e} = u(x_{i}, t_{j})$$
(25)

where $\varphi_i(x)$ and $\varphi_j(t)$ are the one dimensional basis functions. These basis functions consist of Lagrangian interpolants polynomials through the Gauss–Lobatto–Legendre (GLL) collocation points. For example the polynomial $\varphi_j(x)$ defined in the reference domain $\hat{\Omega} = [-1, 1]$ is given by

$$\varphi_j(x) = \frac{(x^2 - 1)\frac{dL_{N_2}(x)}{dx}}{N_2(N_2 + 1)L_{N_2}(x)(x - x_j)}$$
(26)

where the (N_2+1) GLL-points, x_j , are the roots of the first derivative of the Legendre polynomial of degree N_2 , extended with the boundary nodes [5].

4. Wavelet stability analysis

The stability of the system is analyzed by the construction of a non-dimensional stability map. In this work the subcooling and phase-change numbers are used [7]. They correspond with

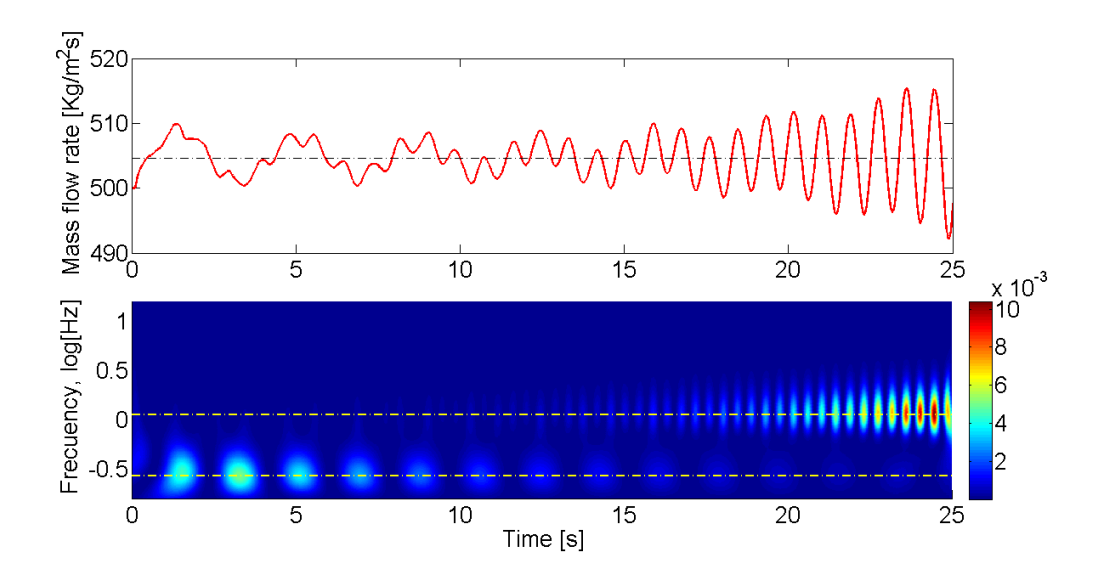


Figure 2: Density wave oscillations and wavelet decomposition. Two different modes can be observed. This case corresponds to the example of section 5.3. The pair (N_{pch}, N_{sub}) for this case is (17,7.5).

$$N_{sub} = \frac{h_f - h_{in}}{h_{fg}} \frac{\rho_{fg}}{\rho_g} \qquad N_{pch} = \frac{Q}{GA_{xs}h_{fg}} \frac{\rho_{fg}}{\rho_g}$$
 (27)

To evaluate the stability of the numerical solution the evolution of the inlet flow is analyzed by using wavelet decomposition [2]. In particular the "Mexican hat" wavelets family is used. This analyzing technique is useful not just to analyze the frequency spectrum but also to obtain the evolution of this spectrum. In Figure 2 the wavelet decomposition of a simulated case is presented. The color-bar corresponds with the percentage of energy for each coefficient of the wavelet decomposition. In this case the decomposition is characterized by two peaks at different frequencies. The lower frequency component behaves in convergent fashion, while the high frequency component evolve with a divergent behavior. The peak position for each characteristic frequency, F_i , is detected and an exponential curve is fitted to the maximum values of the wavelet decomposition evolution at this particular frequency. Then according to the obtained exponential function, $f(t) = Ae^{-\alpha t}$, the stability criterion for each mode corresponds to eq. (28). In this way the wavelet analysis allow to analyze independently the evolution of different frequency modes.

$$\alpha > 0$$
 Stable $\alpha < 0$ Unstable (28)

5. Numerical Results

All the simulations in this section are done in a system with the following characteristics:

- Fluid: R134a
- $L_{TS} = 1$ m, $D_H = 5$ mm
- $K_{in} = 10$, $K_{out} = 1$

The numerical order of approximation of time and space is 4. The number of elements in which the space is discretized is $N_e = 50$ and the time step is $\Delta t = 10^{-2}$ sec for all the cases. The non-linear relative error for the Picard loop is fixed in 10^{-6} .

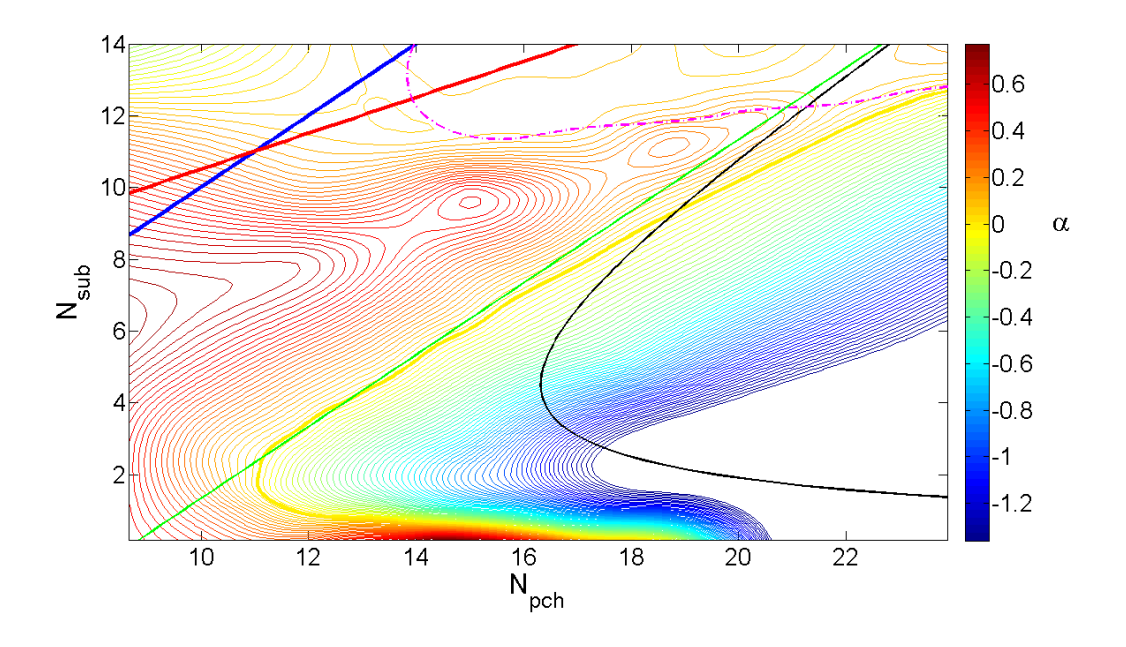


Figure 3: Stability map for $L_{in} = L_{out} = 0$. This stability map corresponds to the normal DWO mode. Green and black lines are, respectively, Ishii's simplified correlation [7] and Guido's correlation [6]. Rose line and red lines show the numerical stability limit and Guido's criterion for the occurrence of Ledinegg instability.

5.1. No external inertia

In this example a no external inertia case is analyzed, $L_{in}=0$ and $L_{out}=0$. the corresponding stability map is presented in Figure 3. A total of 204 cases have been used for the construction of this map. Most of these simulations are localized close to the stability limit to assure an accurate description of the system in that region. Ishii's and Guido's stability criteria for DWO are plotted in this figure. Guido's prediction does not describe the limit of stability in an accurate way. The difference is probably due to the simple lumped model used by Guido to obtain that limit. In contrast in the case of Ishii's criterion the stability limit is predicted more accurately. Nevertheless for high subcooling this simplified criterion and the numerical limit does not agree. One of the main differences of the model used in this work and previous works is that the density profile is updated in each non-linear step as a function of the enthalpy profile. Moreover the numerical limit and Guido's correlation for the occurrence of Ledinegg excursions is also plotted (rose line and red line). The predicted limit differs significantly of the numerical obtained limit. Therefore the usage of Guido's limit, for both Ledinegg and DWO, to real cases should be very carefully analyzed, since this criteria does not seem to reflect the nature of the involved phenomena. While Ishii's limit seems to predict properly and conservatively the occurrence of DWO. None high-order modes are observed in the analyzed simulations for this case.

5.2. Inlet inertia

In this example the same case as previously is analyzed using a one meter inlet pipe, $L_{in}=1m$, $L_{out}=0$. 226 numerical simulations have been used to construct the map of Figure 4. Same as before the stability limit criteria for DWO and Ledinegg instabilities are plotted. None of the stability limits seems to predict accurately the DWO stability limit. Since the models used to obtain those limit does not reflect the influence of external parameters as the length of the pipe lines. Moreover the system behaves in a more stable way when inertia is introduced at the inlet of the heated pipe. None high-order modes are observed in this case.

5.3. Outlet inertia

For this case an outlet one meter pipe is considered, $L_{in} = 0$, $L_{out} = 1m$. A total number of 225 cases have been simulated to construct the stability map of Figure 6(a). Ishii's and Guido's stability limits

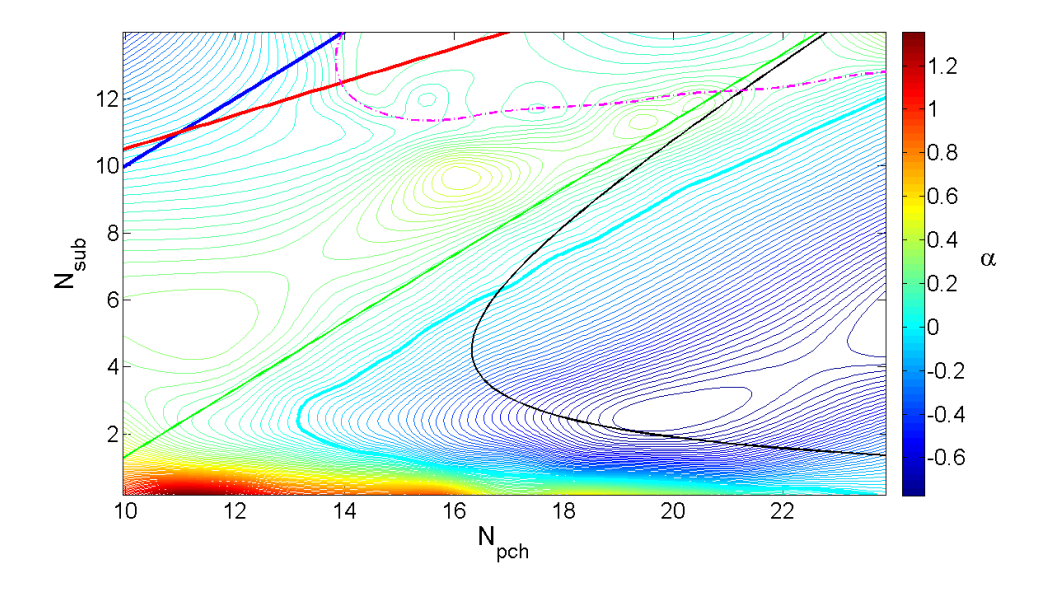


Figure 4: Stability map for $L_{in}=1m$, $L_{out}=0$. This stability map corresponds to the normal DWO mode. Green and black lines are, respectively, Ishii's and Guido's criteria. Rose line and red lines show, respectively, the numerical stability limit for Ledinegg instability occurrence and the Ledinegg Guido's correlation.

for DWO and Ledinegg are also plotted. None of these criteria seem to reflect the stability limit correctly, since none of them take into account external parameters as the inertia of the fluid in non-heated pipes. In contrast with the other two examples, in this case high-order DWO appear for high subcooling. The limits for the normal mode and the high-order modes are plotted in Figures 6(a) and 6(b). For N_{sub} numbers above 5 the high-order modes become unstable even when the natural DWO mode is stable. Moreover for N_{sub} higher than 10 the higher-order oscillations are not a pure frequency oscillation but conversely they correspond to the sum of different frequencies, as shown in Figure 5. This last fact is completely in accordance with the experimental data presented in [15], where for higher subcooling the superposition of higher-modes is observed. The ratio between high-order and normal modes frequencies goes from 2.5 times $(N_{pch} = 14, N_{sub} = 5)$ to approximately 10 times $(N_{pch} = 21, N_{sub} = 12)$.

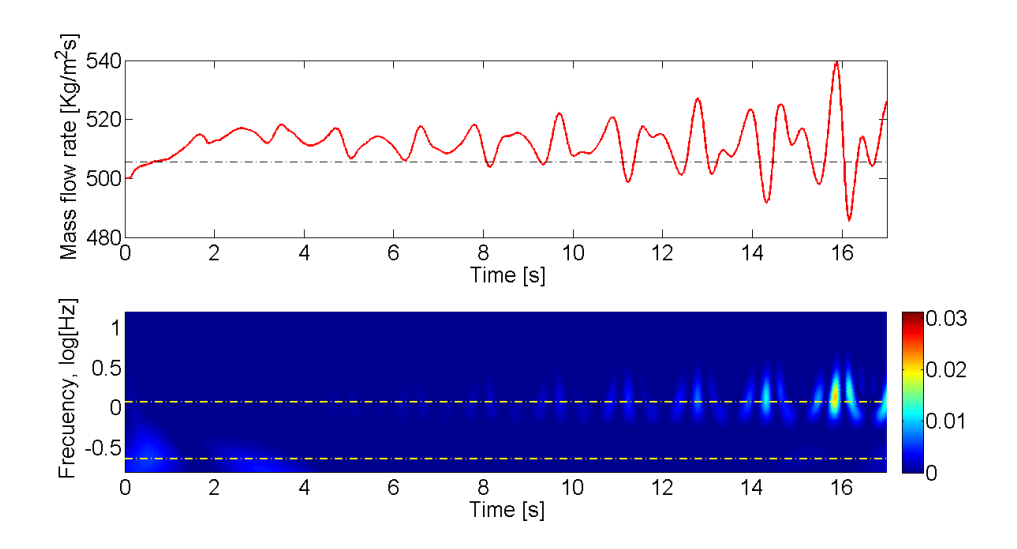


Figure 5: Density wave oscillations and wavelet decomposition. (N_{pch}, N_{sub}) for this case are (19,10.5). In this case the high-order modes are the sum of different frequency components.

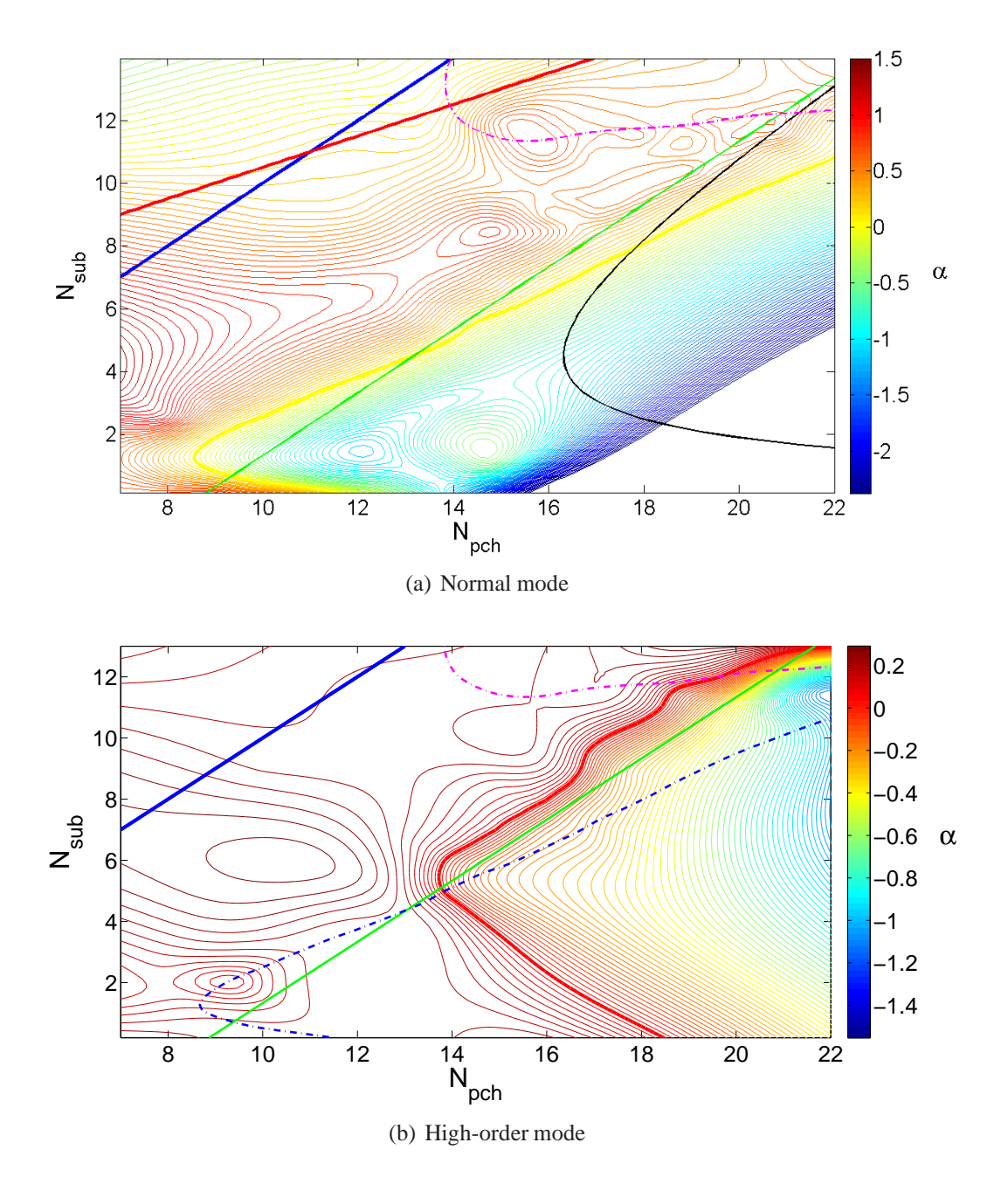


Figure 6: Stability maps for $L_{in}=0$, $L_{out}=1m$. Normal (a) and high-order (b) stability maps are shown. Green and black lines are, respectively, Ishii's and Guido's criteria. Rose line and red lines show the numerical stability limit for Ledinegg instability occurrence and the Ledinegg Guido's correlation.

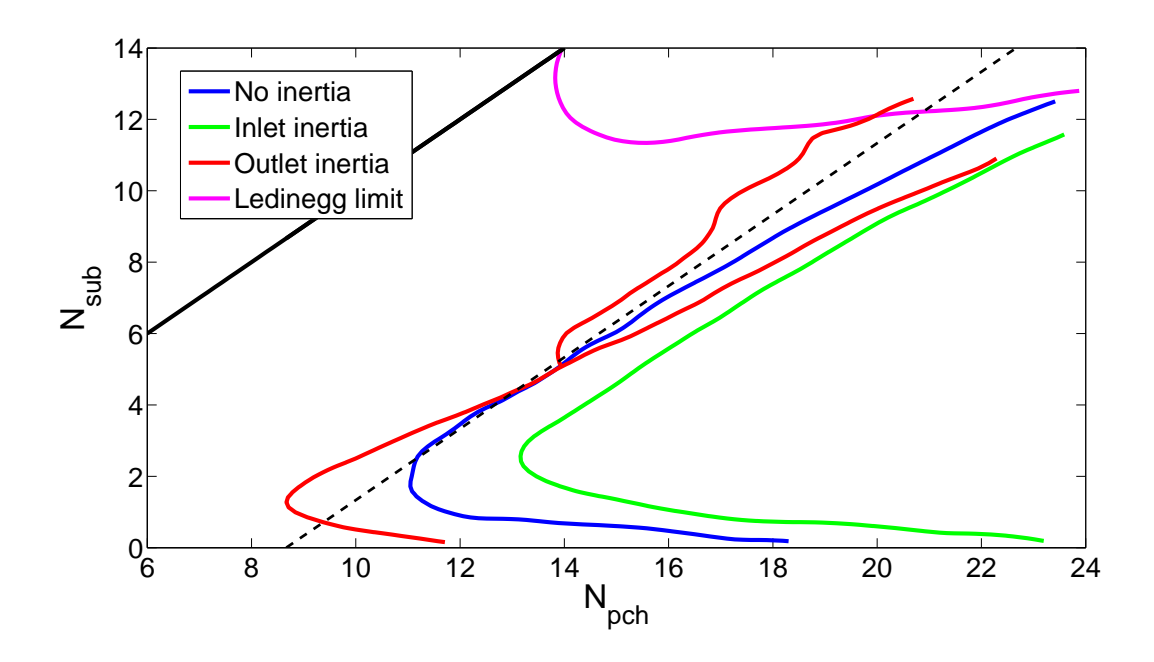


Figure 7: Comparison of the stability limit for the three examples analyzed in this work. No external inertia (blue line), inlet inertia (green line) and outlet inertia (red line). In the case of outlet inertia, higher-modes are observed in the system. The higher-mode stability limit is also plotted in red line.

6. Discussion

In Figure 7 all the stability limits found in this work are plotted. As it is possible to see, the effects of inlet external inertia stabilize the system. In the other hand, outlet inertia not just destabilize the system but also provoke the occurrence of high-order DWO. So according to these conclusions, as an important design rule for two-phase systems, it is possible to say that the outlet pipes (two-phase outlet) should be shortened as much as possible in order to stabilize normal DWO and do not induce high-order modes. Moreover the occurrence of high-order modes can affect more strongly the control systems since their frequency is higher than a normal DWO. The period of the oscillations does not seem to change significantly within the three different examples presented here. In addition, none of the existing stability criteria for DWO predicts the change on the stability limit due to this inertia effects.

The results of this work seem to be the link between Ishii's and Yadigaroglu's works [7, 15]. In those cases it is just necessary to remark that the outlet pipe used in Yadigaroglu's experiment has had a strong influence over the system and has induced high-order modes. In the other hand, in Ishii's experiment the used by-pass configuration allow them to reduce the outlet inertia effects and as a result they do not seen any high-order mode.

Finally the nature of these phenomena should continuing been studied, both experimentally and numerically, to full understand the conditions and parameters that affect the stability. Besides, the prediction of these phenomena in real systems could be improved if the models should better represent all the parameters that can be found in real industrial cases.

7. Conclusions

Density wave phenomenon has been studied in a simple thermal-hydraulic system. The inertia influence of the connecting pipes has been analyzed. It is found that the inlet inertia (longer inlet pipes) increases the stability of the system. On the contrary for the increase of outlet inertia (longer outlet pipes) the stability of the system is not just decreased but also high-order oscillations are induced. The frequency of this high-order oscillations has found to be between 2.5 and 10 times the frequency of the normal mode, according to

 (N_{pch}, N_{sub}) region. Wavelet decomposition has proved to be an efficient analysis technique for this kind of cases where the evolution of different modes is needed.

8. References

- [1] J.-L. Achard, D. Drew, and R. Lahey. The analysis of nonlinear density-wave oscillations in boiling channels. *J. Fluid Mechanics*, 155:213–232, 1985.
- [2] P. S. Addison. *The illustrated wavelet transform handbook*. Institute of Physics Publishing, Bristol, UK, 2002.
- [3] W. Ambrosini, P. Di Marco, and J. Ferreri. Linear and nonlinear analysis of density wave instability phenomena. *International Journal of Heat and Technology*, 18:27–36, 2000.
- [4] W. Ambrosini and J. Ferreri. The effect of truncation error in the numerical prediction of linear stability boundaries in a natural circulation single phase loop. *Nuclear Engineering and Design*, 183(1-2):53–76, 1998.
- [5] M. Deville, P. Fisher, and E. Mund. High-order methods for incompressible fluid flow. *Cambridge University Press.*, 2002.
- [6] G. Guido, J. Converti, and A. Clausse. Density wave oscillations in parallel channels an analytical approach. *Nuclear engineering and Design*, 125:121–136, 1991.
- [7] M. Ishii and N.Zuber. Thermally induced flow instabilities in two-phase. *Proceedings of the forth international heat transfer metting*, 1970.
- [8] R. Lahey and M. Podoski. On the analysis of varius instabilities in two-phase flows. *Multiphase Science and Technology*, pages 183–370, 1989.
- [9] U. Rizwan. Effects of double-humped axial heat flux variation on the stability of two phase flow in heated channels. *Int. J. Multiphase flow*, 20:721–737, 1994.
- [10] U. Rizwan. On density wave oscillations in two-phase flows. *Int. J. Multiphase flow*, 20:721–737, 1994.
- [11] L. Ruspini, C. Dorao, and M. Fernandino. Simulation of a natural circulation loop using a least squares hp-adaptive solver. *Mathematics and Computers in Simulation*, 2010.
- [12] P. Saha, M. Ishii, and N.Zuber. An experimental investigation of the thermally induced flow oscillations in two-phase systems. *Transactions of the ASME*, 1976.
- [13] J. Thome. Engineer Data Book III, chapter 13. Wolverine Tube Inc, 2006.
- [14] F. M. White. Fluid Mechanics. McGraw-Hill, 2003.
- [15] G. Yadigaroglu and A. Bergles. Fundamental and higher mode density-wave oscillations in two-phase flows. *Journal of heat transfer, Trans. ASME*, 94:189–195, 1972.